ELSEVIER

Journal of Physics and Chemistry of Solids 64 (2003) 1395–1403

JOURNAL OF PHYSICS AND CHEMISTRY OF SOLIDS

www.elsevier.com/locate/jpcs

Dilatometric and electrochemical studies on hydrogen transport through RuO_2 coated on palladium

Y. Oren[a,*], A. Tamir[b], Y. Lederman[b], Z. Gavra[c]

[a]*The Institutes for Applied Research, Ben-Gurion University of the Negev, P.O. Box 653, Beer-Sheva 84105, Israel*
[b]*Chemical Engineering Department, Ben-Gurion University of the Negev, P.O. Box 653, Beer-Sheva 84105, Israel*
[c]*Chemistry Department, Nuclear Research Center-Negev, P.O. Box 9001, Beer-Sheva 84190, Israel*

Received 14 February 2003; accepted 8 April 2003

Abstract

Combined electrochemical and dilatometry measurements were used to characterize the transport of hydrogen through thin RuO_2 layers coated on palladium wire electrodes. Hydrogen dissolved in aqueous solutions penetrated through the oxide in a pH-dependent mechanism that combined diffusion of molecular hydrogen and pH-dependent proton hopping through redox sites within the oxide lattice. When cathodically charged, hydrogen was generated and absorbed at the oxide–solution interface only after Ru (IV) reduction occurs, and then, transported into the metal.

Keywords: A. Oxides; A. Metals; D. Diffusion

1. Introduction

The combined electrochemical–dilatometry method applied in this paper was first introduced by the authors as a sensitive tool for studying the kinetic and thermodynamic properties of hydrogen/metal systems [1–3]. With this method, the key principle for studying hydrogen permeation through surface oxides on the metal is that in most such systems changes in the lattice parameters of the base metal are much larger than those in the surface oxide layer in response to hydrogen absorption. Therefore, during the time that hydrogen penetrates through the surface layer, no dimensional variations or only very small variations can be detected.

Only after hydrogen reaches the surface layer–metal interface, and hydrogen absorption by the metal commences, can considerable dimensional changes be detected. The lag times thus obtained provide the basis for calculating characteristic kinetic parameters and deducing the transport mechanism of hydrogen through the surface layer.

In a preceding paper [4], this concept was demonstrated by investigating hydrogen permeation through a thin layer of cerium oxide precipitated on the surface of palladium wire. In those experiments, hydrogen gas was dissolved in aqueous solutions at different pH values. Diffusion coefficients calculated from dilation lag times were not affected by the solution pH. Notwithstanding the fact that cerium oxide is an electrical insulator at room temperature, open circuit potential (OCP) could be measured, and it followed the typical expected trend of palladium upon absorbing or desorbing hydrogen. Accordingly, it was deduced that hydrogen penetrates as a molecule through small pores or imperfections in the cerium oxide lattice.

In the present article, the method was applied for studying hydrogen transport through thin layers of RuO_2 adhering to palladium wire.

RuO_2 has received a great deal of attention over the years because—along with rutile and other rutile-type oxides (e.g. IrO_2)—in single-crystal form it exhibits a near-metal resistivity of $4 \times 10^{-4}\ \Omega$ cm [5,6]. However, it was found [7] that at low-temperatures RuO_2 has resistivities that are

* Corresponding author. Tel.: +972-8-6477167; fax: +972-8-6472960.
E-mail address: yoramo@bgumail.bgu.ac.il (Y. Oren).

0022-3697/03/$ - see front matter © 2003 Elsevier Science Ltd. All rights reserved.
doi:10.1016/S0022-3697(03)00165-3

one to three orders of magnitude larger than this value due to the additional resistance of the crystalline grain boundaries [8]. The high conductivity arises from the fact that the metal–metal distance and the radius of the cation in these oxides are such that overlap of the inner d orbitals is possible and that d electrons in the d bands are responsible for the metallic conduction. This unique property, along with the relatively high chemical stability and catalytic activity of RuO_2, has stimulated the interest in this group of oxides. RuO_2, in particular, has been extensively investigated and is in wide use as a catalytic coating for electrodes in chlorine-alkali cells [9–11].

RuO_2 is also used as a charge storage material in electrochemical 'supercapacitors' [12–14]. These capacitors are based on the double-layer capacitance of high-surface-area electronic conductors (e.g. carbon) or on the pseudo-capacitance of transition metal hydrous oxides such as $RuO_2{\cdot}x\,H_2O$. This capacitance arises mainly from a 3D successive electron transfer at the multi-redox centers, Ru(II) ⇔ Ru(III) ⇔ Ru(IV), balanced by conversion of OH^- to O^{2-} via proton transfer. It is therefore proton migration through the oxide structure that is essential for the mechanism of pseudo-capacitance charging [15]. Accordingly, Jow and Zheng [14] found that hydrogenation of amorphous $RuO_2{\cdot}x\,H_2O$ to $H_{0.43}RuO_2{\cdot}x\,H_2O$ is indeed possible, leading to doubling of the specific capacitance as a result of an increase in the number of Ru atoms involved in the redox chain. On the other hand, crystalline RuO_2 did not exhibit high capacity. These unique characteristics of hydrous and anhydrous, crystalline and amorphous, RuO_2 have been exploited in a number of studies to elucidate the mechanisms involved in charge transfer and to determine the kinetic parameters of such systems. In one such study, Weston and Steele [16] using a potential step technique, found the diffusion coefficient of protons in a chlorine-doped RuO_2 powder to be one order of magnitude smaller than that of a pure RuO_2 powder. These results were consistent with those for oxide thin films prepared under similar conditions. Rishpon and Gottesfeld [17] used elipsometry and AC impedance measurements to study the mechanism of proton conduction within anodic oxide films formed on Ru and within oxide films formed by thermal decomposition of $RuCl_3$. They reported that H^+ transport consists of a fast step, attributed to charging at the grain surfaces, and a slower mode that apparently involves incorporation of aqueous protons into the oxide grains with a characteristic diffusion coefficient of 10^{-11}–$10^{-12}\,cm^2\,s^{-1}$. In an investigation of the electrochemical behavior of a thin RuO_2 layer on Ti in acidic solutions at a potential range between hydrogen and oxygen evolution, Doblhofer et al. [18] found that oxidation state of surface Ru varied from +2 to +6. Since coulometric measurements facilitate separation between surface and bulk processes, these authors estimated the volume diffusion coefficient of hydrogen to be $10^{-19}\,cm^2\,s^{-1}$. Considering the stability of the oxide film, they concluded that grain boundary diffusion is favored in this specific case.

Hydrogen transport has also been studied with respect to other rutiles. Pyun et al. [19], for example, measured the diffusion coefficient of protons through a plasma-enhanced chemical-vapor-deposited TiO_2 layer on Pd by the lag-time method and AC impedance spectroscopy. The low diffusion coefficient values measured led them to conclude that hydrogen transport was hindered due to trapping of the hydrogen within the oxide lattice. These conclusions are supported by an earlier work of Ginley and Knotek [20], who found that hydrogen may occupy two different sites within a rutile: in one type, interaction with surface oxygen is involved and in the other, lattice defects play an important role.

In the present article, hydrogen transport through thin RuO_2 layers is investigated under open and closed circuit conditions in acidic and basic solutions.

2. Experimental

The experimental setup for simultaneous measurements of dimensional changes and electrochemical properties is described in detail elsewhere [2,3]. In the present case, palladium wires coated with a RuO_2 layer were used as the working electrodes. Two types of hydrogen source were used: either hydrogen generated by cathodic water reduction at the oxide–solution interface (which is facilitated by the electronic conductivity of the oxide) or gaseous hydrogen bubbled through the solution. Maximum hydrogen solubility (6.6×10^{-4} and $5.3\times10^{-4}\,mol\,l^{-1}$ in 1N H_2SO_4 and 1N KOH solutions, respectively, at 25 °C) was reached within a few seconds with the second option. A reversible hydrogen electrode (RHE) was used as the reference electrode for measuring the OCP and the potentials during cathodic charging.

In a typical experiment, a freshly coated palladium wire (0.0127 cm in diameter and typical exposed length of 3.5 cm) was installed in the cell, where it was equilibrated for several hours with 1N H_2SO_4 or 1N KOH. The cell was continuously purged with argon to remove any residual dissolved oxygen. When an external hydrogen source was used, the argon was replaced with gaseous hydrogen bubbled through the solution, while length and OCP variations of the sample were monitored simultaneously. Charging with cathodic hydrogen was performed galvanostatically while maintaining a slow argon flow above the solution. As was previously performed in our study with cerium oxide [4], the oxide layer was protected from possible damage caused by large and superfluous dimensional changes by terminating the hydrogen flow and starting the argon flow or by disconnecting the current as soon as a slight expansion of the metal was observed.

The lag time for hydrogen transport through the oxide layer was measured as the time difference between the beginning of hydrogen bubbling, or the application of the cathodic current, and the onset of length variations. In both cases, charging with hydrogen was followed by galvanostatic discharge by applying an inverse current density of 1 mA cm^{-2}. As discussed below, slow spontaneous discharge was also observed. However, the galvanostatic discharge was required to expedite the process for preparing the electrode for the next experiment.

Charging with gaseous or cathodically generated hydrogen was also performed for an uncovered palladium wire exposed to the same thermal treatment as the coated wire. The results thus obtained were subtracted from lag time values of the coated electrodes. Lag-time measurements were repeated at least four times for each electrode under each set of experimental conditions. Average values were calculated with a 10–15% standard deviation.

Galvanostatic charging was performed as follows: Oxide-coated or non-coated palladium wire electrodes were exposed to constant cathodic charge densities in the range of 1–4 mA cm^{-2} for different times up to 32 s. Dimensional changes and electrode potential variations were monitored as a function of pulse length. Cyclic voltammograms and galvanostatic charging were performed by a EG&G potentiostate-galvanostate Model 273. Voltage, current, and length variations were monitored by a National Instruments AT-MIO-16 data acquisition setup and LABVIEW software.

2.1. Preparation and characterization of the RuO_2-coated palladium

RuO_2 layers were prepared on palladium wires by thermal decomposition of $RuCl_3$. Prior to this procedure, the palladium surface was washed with acetone in an ultrasound bath to remove any greasy residues. This was followed by dipping the wire in a solution of 1:1 32% HCl and 35% HNO_3 until the light brown color of dissolved $PdCl_2$ appeared. The wire was then washed immediately with deionized water. The treated wire was dipped in a 1 M $RuCl_3$ solution in isopropanol to which concentrated HCl had been added to facilitate solubility. The wet wire was dried at 100 °C for 30 min, followed by thermal decomposition in air at 450 °C for 15 min. This procedure was repeated several times until the desired oxide thickness was reached. The existence of RuO_2 was verified by XRD measurements on palladium foils coated according to the same procedure. An XRD pattern is shown in Fig. 1, along with some typical scattering lines taken from the XRD library. The Pd and RuO_2 lines are clearly visible. The crystalline RuO_2 evident on the X-ray diffractogram may contain significant amounts of the amorphous phase and may also exhibit non-stoichiometry

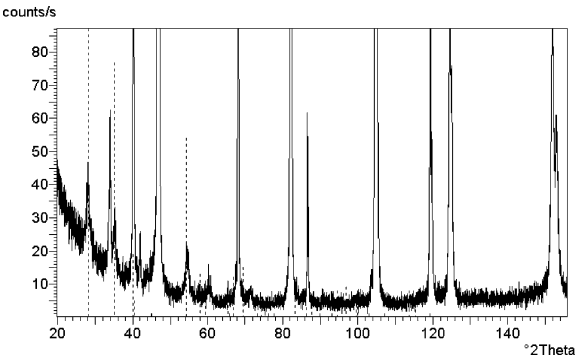

Fig. 1. XRD spectrum of RuO_2 layer on palladium foil; dotted lines relate to RuO_2, all other lines are to Pd.

[7,18,21]. There is also strong evidence for the inclusion of chlorine during the thermal decomposition of $RuCl_3$ [16,22].

The correlation between the thickness of the oxide layer and the number of dipping cycles in the $RuCl_3$ solution was established by dipping a wire coated with two oxide layers in the solution and washing the adhered solution layer with a known volume of water. Repeating this procedure enabled us to determine the concentration of Ru accumulating in the water as a function of the number of dips. The correlation curve thus obtained is shown in Fig. 2. The oxide thickness attributed to a single coated layer is 140 Å, as calculated from the slope of the straight line in Fig. 2, the dimensions of the wire, and a specific gravity of 6.97 g cm^{-3} for RuO_2.

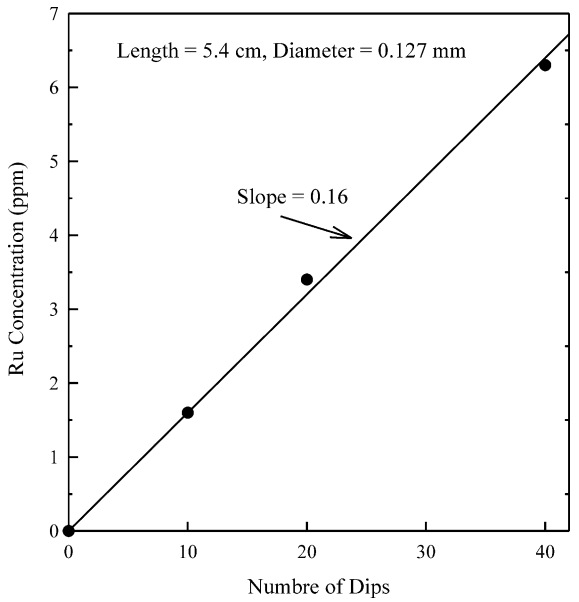

Fig. 2. Calibration curve for RuO_2 layer thickness: ruthenium concentration as a function of the number of dips (see text).

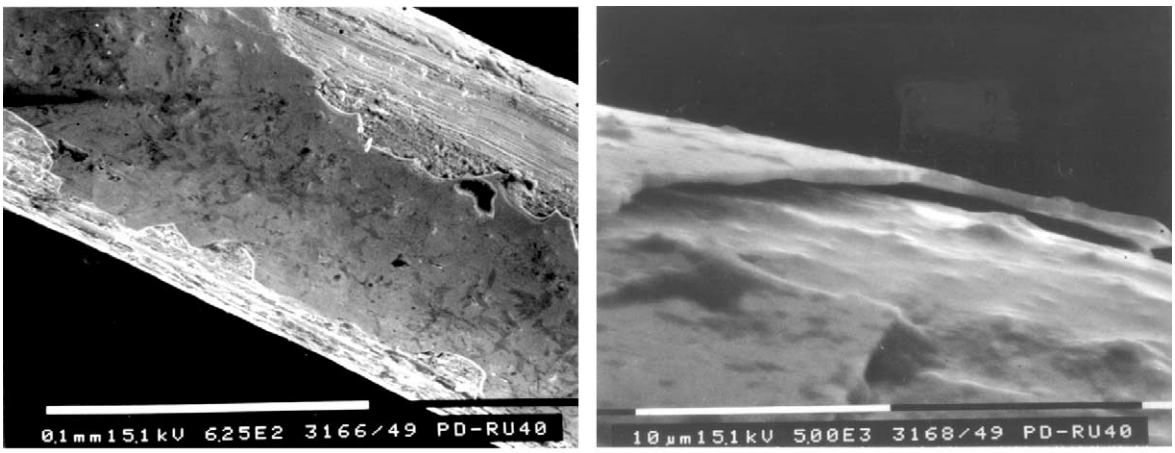

Fig. 3. SEM photographs of a Pd wire coated with RuO_2; (a) × 625; (b) × 5000.

SEM photographs of a coated Pd wire are shown in Fig. 3. In the preparation for these micrographs, the oxide layer was intentionally damaged to facilitate comparative observation between the oxide layer and the palladium substrate. The compactness of the layer is evident from Fig. 3a. The sample shown in Fig. 3b was placed in a normal position underneath the electron beam to facilitate estimation of the thickness of the layer. Good correlation was found between layer thickness calculated according the described calibration and SEM observations on wires coated with multi-layer oxide films.

In this study, samples coated with oxide films of thickness up to 0.56 μm were used. Each freshly prepared sample had to be activated prior to the experiments by charging and discharging with hydrogen. This was done by performing cyclic voltammetry at a sweep rate of 10 mV s^{-1}, in the range +0.1 to +1 V vs. RHE, with simultaneously monitoring changes in the length of the wire. An example of a cyclic voltammogram–dilatogram is given in Fig. 4. Scanning towards the cathodic direction facilitated charging of both the oxide layer and the palladium surface with hydrogen, as can be observed from the reduction current and the subsequent oxidation current signal and from the respective expansion and contraction of the electrode as shown in the dilatogram. The anodic scan was reversed prior to the commencement of oxygen evolution in order to protect the oxide layer. The procedure was repeated until both the voltammograms and the dilatograms reached a constant state. It is believed that this procedure is required to convert the entire layer into a hydrous oxide.

Features that are typical to RuO_2 [7] can hardly be observed in Fig. 4. The reason for this is that in this specific example the oxide layer is too thin to provide RuO_2 redox current signals that are stronger than the palladium background current.

3. Results and discussion

3.1. Charging with dissolved hydrogen gas

Typical behavior of the OCP and the dimensional changes (normalized to the original electrode length) of a palladium wire coated with a 0.56 μm RuO_2 layer during a charging-and-spontaneous-discharge cycle in 1N H_2SO_4 is depicted in Fig. 5a. An expanded view of the behavior at the very beginning of the charging process under the same conditions is shown in Fig. 5b. In general, similar patterns were observed with coated electrodes in 1N KOH and with non-coated electrodes in 1N KOH and H_2SO_4. However, the following important differences

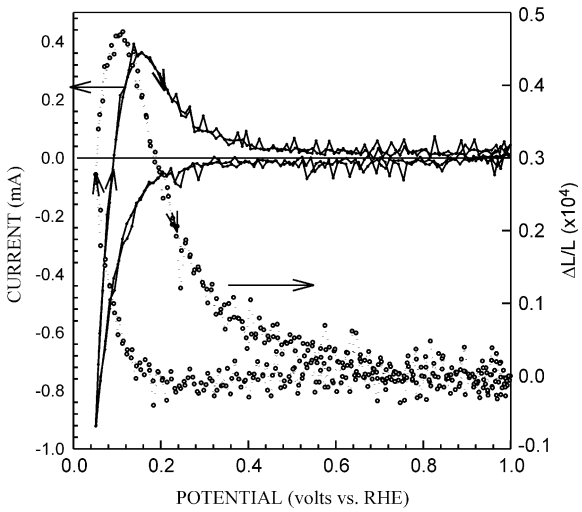

Fig. 4. Voltammogram and dilatogram for Pd(RuO_2/0.28 μm) electrode in 1N H_2SO_4. Sweep rate 10 mV s^{-1}.

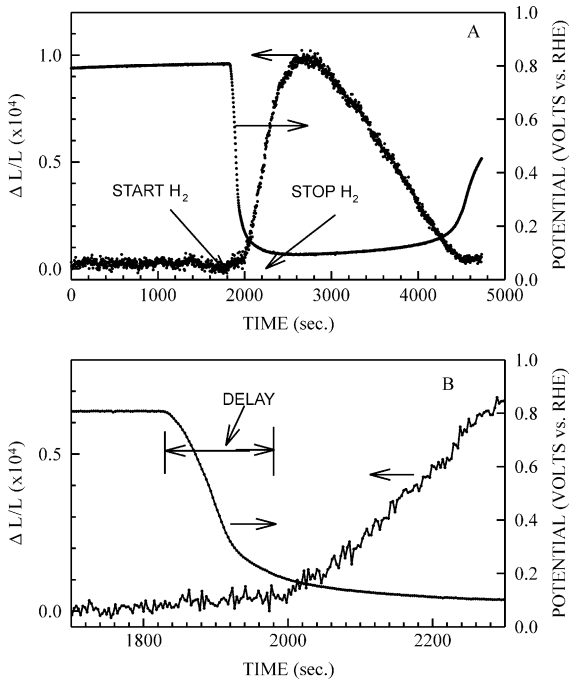

Fig. 5. (a) Length and OCP changes of Pd wire coated with 0.56 μm RuO_2 during charging with gaseous hydrogen dissolved in 1N H_2SO_4. Discharge is spontaneous. (b) Expanded view of the early charging stage.

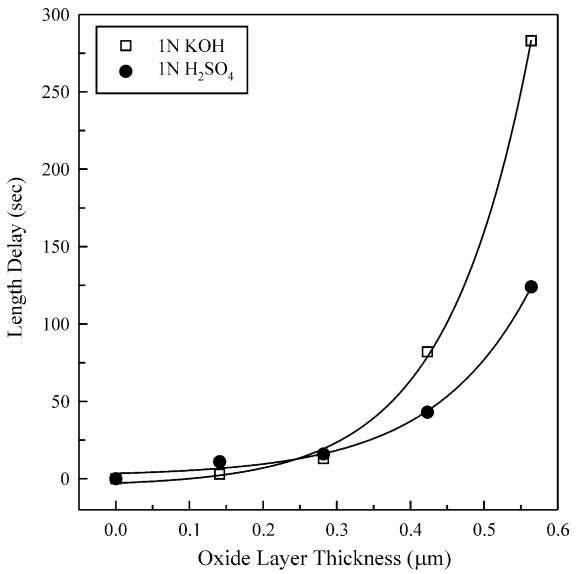

Fig. 6. Lag time as a function of the oxide layer thickness in acidic and basic solutions resulting from charging with dissolved gaseous hydrogen.

were evident: Firstly, both OCP and length variations were significantly slower for the coated wire than for the non-coated palladium. Secondly, in both coated and non-coated palladium, the time gap between the beginning of hydrogen bubbling and the onset of length and OCP variations ('lag time') was considerably shorter in acid than in basic solution. Thirdly, spontaneous discharge of the coated palladium started as soon as hydrogen bubbling was stopped, as was evident from the electrode contraction as conditions changed. Similar behavior was previously observed for a Pd–CeO_2 system [4]. In contrast, hydrogen charged bare palladium electrodes showed much slower spontaneous discharge than coated electrodes.

Net lag times (i.e. after deducting lag times measured with a bare palladium wire under the same conditions) are summarized in Fig. 6 as a function of the oxide layer thickness for the acid and base solutions. It is evident that for layer thickness of ≤ 0.3 μm, lag times are apparently insensitive to the solution pH. However, as the thickness exceeds 0.3 μm, lag times measured in the acid solution were significantly shorter than those obtained with the base. To explain this behavior, it may be suggested that hydrogen transport through the RuO_2 layer is driven by two mechanisms: (1) diffusion of dissolved molecular hydrogen through small defects within the layer, and (2) proton hopping facilitated by pH-dependent redox interactions through sites located within the RuO_2 lattice. The explanation must be viewed in terms of the multi-step procedure used for the preparation of the oxide layer of the desired thickness. It is assumed that at thickness values <0.3 μm molecular diffusion predominates, probably as a result of the layers not yet being sufficiently compact and therefore having pores that are large enough to allow free diffusion of molecular hydrogen towards the oxide–metal interface. As new layers are formed on the top of the old ones, the latter may become much more compact due to absorption of the reaction solution, and additional oxide mass may form within the pores during thermal decomposition. As the layers become sufficiently thick, free diffusion of molecular hydrogen becomes less important, and the proton-jumping mechanism dominates, leading to pH-dependent lag times, as shown in Fig. 6.

It is possible that the stepwise pH-dependent proton transport may take place via the following mechanism:

(i) Dissociative adsorption of dissolved hydrogen molecule at the hydrous oxide–solution interface:

$$H_2 + 2RuO_2(H_2O)_y \leftrightarrow 2RuO_2(H_2O)_y \cdot H_{ads.} \quad (1)$$

(ii) Protonation of adsorbed hydrogen atoms at sub-interfacial oxide sites:

$$2RuO_2(H_2O)_y \cdot H_{ads.} \leftrightarrow 2RuO_2(H_2O)_y + 2H^+ + 2e \quad (2)$$

(iii) Redox-facilitated proton transport through sites within the hydrous oxide lattice:

$$2RuO_2(H_2O)_y + 2H^+ + 2e \leftrightarrow 2RuOOH(H_2O)_y \quad (3.1)$$

in basic solution and

$$2RuO_2(H_2O)_y + 2H^+ + 2e \leftrightarrow Ru_2O_3(H_2O)_{y+1} \quad (3.2)$$

in acidic solution.

In fact, reactions (3.1) and (3.2) constitute a state of equilibrium between a 'free' (H^+) and an 'immobilized' (RuOOH or H_2O) proton within the oxide. Similar stepwise mechanisms for electrochemically driven H transport have been proposed in previous studies [23–25].

(iv) Proton–electron recombination at the oxide–metal interface:

$$2H^+ + 2e \leftrightarrow 2H^{\cdot} \quad (4)$$

This step is then followed by the well-established mechanism of hydrogen penetration into metals [26], namely, adsorption of hydrogen atoms on the metal surface, followed by their absorption into a sub-interfacial metal layer and diffusion through the metal lattice, resulting in dimensional changes.

It may be assumed that reactions (1)–(4) are reversible, and therefore each is characterized by both a forward and backward rate constant. However, the results of the lag-time studies shown in Fig. 6 do not provide information on the contribution of each separate reaction. Thus, it is not possible to obtain each specific rate constant separately. However, since reactions (1), (2) and (4) are interfacial processes, it is safe to assume that they do not contribute to the dependence of the lag time on the oxide thickness and the rate-determining processes are those taking place within the oxide bulk, namely, reactions (3.1) and (3.2). If these reactions are sufficiently rapid, then a local equilibrium will exist between the free and immobilized hydrogen species within the oxide layer. It is apparently this partial immobilization that leads to the hindered and pH-dependent diffusion of hydrogen within the oxide lattice.

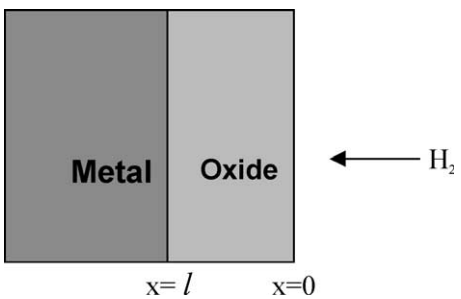

Fig. 7. Schematic representation for the transport model in the oxide–metal system.

Keeping in mind the assumptions made above with regard to the two thickness regions, we may determine the diffusion coefficient of molecular hydrogen and the hindered diffusion coefficients as follows. We assume the transport model shown schematically in Fig. 7. The time-dependent transport equation is solved for a planar sheet (we may adopt this geometry because the thickness of the oxide layer is much smaller than the diameter of the wire [4]), and the lag-time expression is solved by the method of Crank [27], taking into account the appropriate initial and boundary conditions, namely:

$$t = 0 \qquad C = 0 \quad (5a)$$

$$t > 0 \qquad X = 0 \;\; C = 0 \quad (5b)$$

$$t > 0 \qquad X = 1 \;\; C = C_0 \quad (5c)$$

Condition (5b) is justified by the fact that diffusion of hydrogen within the metal is much faster than that in the oxide [19]. Therefore, at the very early stages of charging the metal with hydrogen, its flux into the metal is high, and therefore each hydrogen atom is transported to the palladium bulk immediately upon reaching the oxide–metal interface. The solution provides the following expressions for the lag time t_d

$$t_d = \frac{l^2}{6D_{H_2}} \quad (6)$$

for $l < 0.3$ μm and

$$t_d = \frac{l^2}{6D_{acid}} \text{ or, } t_d = \frac{l^2}{6D_{base}} \quad (7)$$

for $l > 0.3$ μm.

D_{H_2} denotes the diffusion coefficients for H_2 in the region $l < 0.3$ μm, D_{acid} and D_{base}, the diffusion coefficient in the acid and base, respectively, when $l > 0.3$ μm, and l, the layer thickness. Consequently, by fitting expressions (6) and (7) to the results in the appropriate thickness regions in Fig. 6, the following calculated diffusion coefficients are obtained: $D_{H_2} = 9.5 \times 10^{-12}$ cm^2 s^{-1}, $D_{acid} = 1.22 \times 10^{-12}$ cm^2 s^{-1} and $D_{base} = 5.03 \times 10^{-13}$ cm^2 s^{-1}. The values for D_{acid} and D_{base} actually reflect the situation in which hydrogen 'immobilization' is preferred in the basic solution, leading to more hindered diffusion.

3.2. Charging with electrochemically generated hydrogen

Cathodic reduction of water on the interfaces of metals and conductive oxides follow the well-known Volmer–Heyrovsky–Tafel scheme [28]. In addition, when charged cathodically, hydrous Ru(IV) may undergo a series of reduction reactions to produce to a mixture of Ru(IV), Ru(III) and Ru(II) [23,18]. According to Doblhofer et al. [18], the bulk phase of a RuO_2 film remains intact while reduction occurs mostly on the oxide surface that is exposed

to the solution. That is because the surface groups are less thermodynamically stable. The redox transitions make the Ru adsorption sites more susceptible for interaction with protons to form adsorbed hydrogen upon reaching the proper cathodic potential.

Thus, the following general irreversible cathodic surface reactions may be suggested:

$$RuO_{(x+\delta)}(H_2O)_{(y-\delta)} + \delta e + \delta H_2O \rightarrow RuO_x(H_2O)_y \cdot \delta H_{ads.} + \delta OH^- \quad (8)$$

in basic solutions, and,

$$RuO_{(x+\delta)}(H_2O)_{(y-\delta)} + (2\delta+1)H^+ + (2\delta+1)e \rightarrow RuOx(H_2O)_y \cdot H_{ads.} \quad (9)$$

in acidic solutions.

When a perfectly compact oxide layer is considered, it is likely that hydrogen atoms adsorbed at the oxide–solution interface reach the metal support through a series of reversible redox transitions similar to that described for the dissolve hydrogen (Eqs. (3.1) and (3.2)). However, as the oxide layer may contain micro-fissures and pores, surface groups that are exposed to the solution and undergo reactions (8) or (9) could be present even in the oxide 'bulk'. Thus, the existence of adsorbed hydrogen in the vicinity of the oxide–palladium surface should be taken into account. This should result in a much shorter diffusion time of hydrogen towards the metal as compared to that from the outer oxide interface.

Typical dimensional changes for a coated electrode at different current densities and exposure times are shown in Fig. 8. The linear dependence of length variations with time enabled to obtain a lag-time value for each current density by extrapolating to $\Delta L/L = 0$. Net lag times thus obtained are expressed as function of the oxide thickness and current density in Figs. 9 and 10 for the base and acid, respectively. It is evident that the pattern of lag times shown in these figures differs from that resulting from charging with dissolved gaseous hydrogen: the values of the former lag times are an order of magnitude smaller and they behave linearly as a function of the oxide layer thickness. Nevertheless, as in the case for charging with dissolved hydrogen, lag times in the present case are much shorter under acidic conditions.

The linear behavior of the lag times with respect to the oxide layer thickness and their somewhat small values suggest that in this case diffusion processes play a minor role for hydrogen transport towards the metal. In the light of the discussion above, the lag times resulting from the cathodic charging are due to the time required for reducing the hydrous oxide surface groups, both at the oxide–solution interface and in internal surface created by micro-fissures and pores. The concentration of these groups is directly related to the amount of oxide deposited on the metal. Hydrogen is formed and absorbed on the surface within

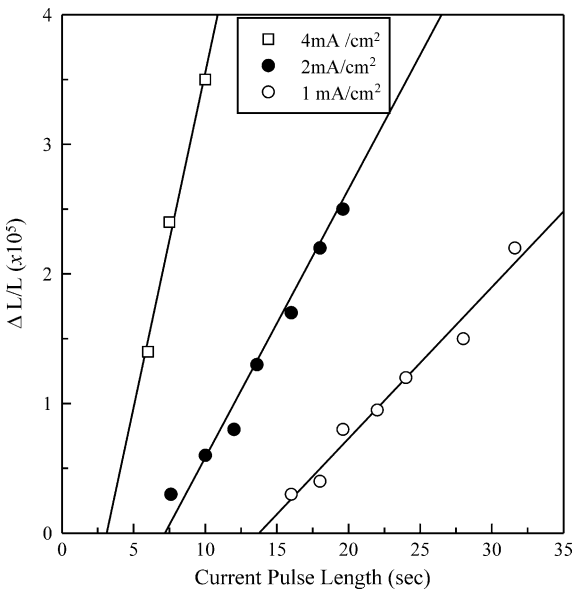

Fig. 8. Galvanostatic charging in 1N KOH: strain as a function of current pulse time for different current densities. RuO_2 thickness is 0.56 μm.

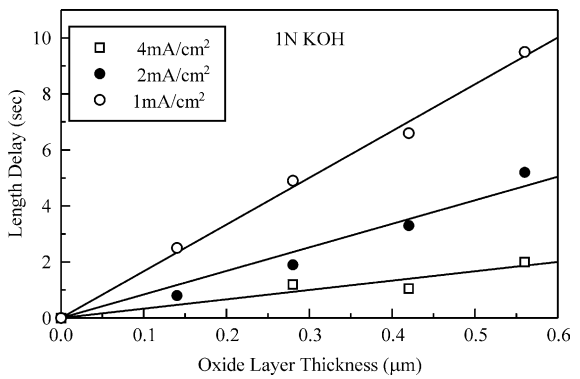

Fig. 9. Net lag time as a function of RuO_2 thickness and current density in 1N KOH.

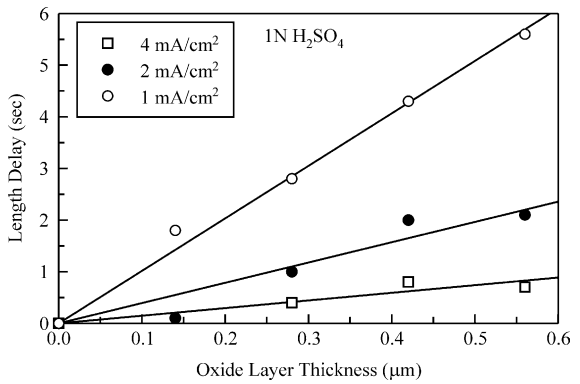

Fig. 10. Net lag time as a function of RuO_2 thickness and current density in 1N H_2SO_4.

Table 1
Diffusion coefficients of hydrogen in thin-layer rutiles—literature summary

Oxide	Diffusion coefficient $cm^2\ s^{-1}$	Conditions
RuO_2	5×10^{-14}	700 °C treated oxide, cold pressed powder, proton diffusion in 1.2N HCl, potential step method [16]
RuO_2	5.2×10^{-15}	450 °C treated oxide, cold pressed powder, proton diffusion in 1.2N HCl, potential step method [16]
RuO_2	$10^{-11}-10^{-12}$	AC impedance in 0.5 M H_2SO_4, proton diffusion, anodic oxidation of Ru on gold or $RuCl_3$ thermal decomposition on gold [17]
RuO_2	$D_{H_2}=9.5\times10^{-12}$ $D_{acid}=1.2\times10^{-12}$ $D_{base}=5.0\times10^{-13}$	This work
TiO_2	$(3.9-5.2)\times10^{-14}$	Oxide on Pd, cathodic charging in 0.1N NaOH, time-lag method, 'hydrogen' diffusion [19]
TiO_2	$(3.4-17)\times10^{-11}$	Oxide on Pd, AC impedance in 0.1N NaOH, 'hydrogen' diffusion [29]

the bulk of the oxide layer and near the oxide–palladium interface only when UPD conditions for hydrogen are reached. The fact that no diffusion type transport of hydrogen was observed suggest that the immediate source for hydrogen to be absorbed within the metal is that formed at the vicinity of the metal–oxide interface.

4. Summary and conclusions

Despite the large number of studies devoted to the interaction of hydrogen with ruthenium dioxide, only a few have been dedicated to hydrogen transport properties, particularly through thin oxide layers. A summary of diffusion data for RuO_2 and TiO_2 available in the literature and the values obtained in this work is presented in Table 1. The data presented in Table 1 reveal large discrepancies in the values measured by different authors for the diffusion coefficient of hydrogen in thin layers of RuO_2 and TiO_2. The values vary, presumably not only due to different preparation procedures and measuring conditions but also, paradoxically, due to the choice of the measuring method (as for TiO_2) for (apparently) similarly prepared samples. We are led to the conclusion that the diffusion of hydrogen through rutiles is extremely sensitive to variations in the experimental conditions under which the measurements are performed and these should therefore be carefully controlled. Two additional aspects of this subject are emphasized in this article, namely, the importance of the hydrogen source and that of the physical and chemical properties of the oxide layer.

Acknowledgements

The study was supported by the Israel Council for Higher Education and the Israel Atomic Energy Commission. The authors wish to thank Ms H. Sela and Dr G. Kimmel for preparing XRD samples and interpreting the XRD results.

References

[1] Z. Gavra, M. Abda, Y. Oren, in: F. Lapicque, A. Stork, A.A. Wragg (Eds.), Electrochemical Engineering and Energy, Plenum Press, New York, 1994.
[2] Y. Oren, E. Elish, A. Tamir, Z. Gavra, J. Alloys Compd. 235 (1996) 30.
[3] E. Elish, Electrochemical–dilatometry characterization of metals and metal alloys for hydrogen storage and gettering, MSc Thesis, Ben-Gurion University of the Negev, Beer-Sheva, August 1996
[4] Y. Oren, A. Tamir, Y. Lederman, Z. Gavra, J. Phys. Chem. Solids 63 (2002) 57–64.
[5] W.D. Ryden, A.W. Lawson, C.C. Sartain, Phys. Lett. 26A (1968) 209.
[6] H. Schafer, G. Schneidereit, W. Gerhardt, Z. Anorg, Allgem. Chem. 372 (1963) 319.
[7] S. Trasatti, G. Lodi, in: S. Trasatti (Ed.), Electrodes of Conductive Metallic Oxides, Part A, Elsevier, New York, 1980, p. 301.
[8] S.R. Morrison, The Chemical Physics of Surfaces, Plenum Press, New York, 1977, p. 69.
[9] D. Galizzioli, F. Tantardini, S. Trasatti, J. Appl. Electrochem. 4 (1974) 57.
[10] S. Trasatti, G. Buzzanca, Electroanal. Interfacial Electrochem. 29 (1971) App. 1.
[11] O. De Nora, Chem. Engng Technol. 42 (1970) 222.
[12] B.E. Conway, J. Electrochem. Soc. 138 (6) (1991) 1539.
[13] J.P. Zheng, T.R. Jow, J. Electrochem. Soc. 142 (1) (1995) L6.
[14] T.R. Jow, J.P. Zheng, J. Electrochem. Soc. 145 (1) (1998) 49.
[15] H. Hadzi-Jordanov, H. Angerrstein-Kozlowska, M. Vukovic, B.E. Conway, J. Electrochem. Soc. 125 (1978) 1471.
[16] J.E. Weston, B.C.H. Steele, J. Appl. Electrochem. 10 (1980) 49.
[17] J. Rishpon, S. Gottesfeld, J. Electrochem. Soc. 131 (8) (1984) 1960.

[18] K. Doblhofer, M. Metiikos, Z. Ogumi, H. Gerischer, Ber. Bunsenges. Phys. Chem. 82 (1978) 1046–1050.
[19] S.I. Pyun, J.W. Park, Y.G. Yoon, J. Alloys Compd. 231 (1995) 315.
[20] D.S. Ginley, M.L. Knotek, J. Electrochem. Soc. 126 (12) (1975) 2163.
[21] D. Galizzioli, F. Tantardini, S. Trasatti, J. Appl. Electrochem. 5 (1975) 203–214.
[22] S. Pizzini, G. Buzzanca, C. Mari, L. Rossi, S. Torchio, Mater. Res. Bull. 7 (1972) 449–462.
[23] D. Michell, A. J. Rand, R. Woods, J. Electroanal. Chem. 89 (1978) 11–27.
[24] S. Ardizzone, G. Fregonara, S. Trasatti, Electrochim. Acta 35 (1990) 263.
[25] J.P. Zheng, P.J. Cygan, T.R. Jow, J. Electrochem. Soc. 142 (8) (1995) 2699.
[26] F. Waelbroeck, Influence of bulk and surface phenomena on the hydrogen permeation through metals, ISSN 0366-0885, Julich GmbH Publication 1966, December 1984
[27] J. Crank, The Mathematics of Diffusion, Oxford University Press, Oxford, 1967, pp. 47–49, 121–124.
[28] K.J. Vetter, Electrochemical Kinetics, Academic Press, New York, 1967.
[29] Y.G. Yoon, S.I. Pyun, Electrochim. Acta 40 (8) (1995) 999.